

DISCOVERY OF AN ULTRASOFT X-RAY TRANSIENT SOURCE IN THE 2XMM CATALOG: A TIDAL DISRUPTION EVENT CANDIDATE

DACHENG LIN¹, ELEAZAR R. CARRASCO², DIRK GRUPE³, NATALIE A. WEBB¹, DIDIER BARRET¹, AND SEAN A. FARRELL⁴

Draft version January 27, 2013

ABSTRACT

We have discovered an ultrasoft X-ray transient source, 2XMMi J184725.1-631724, which was detected serendipitously in two *XMM-Newton* observations in the direction of the center of the galaxy IC 4765-f01-1504 at a redshift of 0.0353. These two observations were separated by 211 days, with the 0.2–10 keV absorbed flux increasing by a factor of about 9. Their spectra are best described by a model dominated by a thermal disk or a single-temperature blackbody component (contributing $\gtrsim 80\%$ of the flux) plus a weak power-law component. The thermal emission has a temperature of a few tens of eV, and the weak power-law component has a photon index of ~ 3.5 . Similar to the black hole X-ray binaries in the thermal state, our source exhibits an accretion disk whose luminosity appears to follow the $L \propto T^4$ relation. This would indicate that the black hole mass is about 10^5 – $10^6 M_\odot$ using the best-fitting inner disk radius. Both *XMM-Newton* observations show variability of about 21% on timescales of hours, which can be explained as due to fast variations in the mass accretion rate. The source was not detected by *ROSAT* in an observation in 1992, indicating a variability factor of $\gtrsim 64$ over longer timescales. The source was not detected again in X-rays in a *Swift* observation in 2011 February, implying a flux decrease by a factor of $\gtrsim 12$ since the last *XMM-Newton* observation. The transient nature, in addition to the extreme softness of the X-ray spectra and the inactivity of the galaxy implied by the lack of strong optical emission lines, makes it a candidate tidal disruption event. If this is the case, the first *XMM-Newton* observation would have been in the rising phase, and the second one in the decay phase.

Subject headings: accretion, accretion disks — galaxies: individual:2XMMi J184725.1-631724 — galaxies: nuclei — X-rays: galaxies.

1. INTRODUCTION

It is generally believed that supermassive black holes (SMBHs) reside in many galaxies, but only a fraction of them exhibit active galactic nuclei (AGN), while others are dormant (Kormendy & Richstone 1995). Tidal disruption events can provide a unique way to find and study the dormant SMBHs (Rees 1988). Such an event occurs when a star approaches a SMBH and is tidally disrupted and subsequently accreted (Lidskii & Ozernoi 1979; Rees 1988). The mass of the SMBH should be $\lesssim 10^8 M_\odot$ for such events to occur outside the event horizon for solar-type stars. Tidal disruption events are expected to be transient and rare, with the average occurrence rate of $\sim 10^{-4} \text{ yr}^{-1}$ per galaxy (Rees 1990). They are predicted to have a fast rise, with a timescale of half a year, and the decay can last on the order of months to years, with the luminosity decaying as $L \propto t^{-5/3}$ (Lidskii & Ozernoi 1979; Rees 1988, 1990). The peak of the flare is expected to reach the Eddington luminosity and be dominated by thermal UV or X-ray emission.

A few tidal disruption event candidates were found from the *ROSAT* All-Sky Survey, such as

RX J1624.9+7554, RX J1242.6-1119 and NGC 5905 (Grupe et al. 1999; Komossa & Greiner 1999; Komossa & Bade 1999). Their host galaxies were confirmed to be inactive or only weakly active (NGC 5905) using *Hubble Space Telescope* spectroscopy (Gezari et al. 2003). They had peak soft X-ray luminosities up to $\sim 10^{44} \text{ erg s}^{-1}$ and showed ultrasoft X-ray spectra with blackbody temperatures of ~ 0.04 – 0.1 keV (Komossa 2002, 2008). NGC 5905 is the best observed candidate and is the first one found to follow approximately the $L \propto t^{-5/3}$ evolution. Some candidates were detected recently from the *XMM-Newton* Slew Survey (Esquej et al. 2007, 2008) in the X-rays and from the *Galaxy Evolution Explorer* Deep Imaging Survey in the UV (Gezari et al. 2006, 2008, 2009). Very recently, the transient source Swift J164449.3+573451 was suspected to be due to a tidal disruption event (Bloom et al. 2011; Burrows et al. 2011). In contrast with the candidates above and the theoretical prediction, this source is hard in X-rays, with a photon index around 1.8 (Burrows et al. 2011). Its tidal disruption event explanation still needs to be confirmed by future long-term monitoring.

We are carrying out a project of classifying a sample of sources in the Second *XMM-Newton* Serendipitous Source (2XMM) Catalog (Watson et al. 2009). Here we report on the discovery of an ultrasoft X-ray transient source, 2XMMi J184725.1-631724, whose position is RA=18:47:25.16, Dec=−63:17:24.96 (J2000) from the 2XMM catalog, with a $1\text{-}\sigma$ error of $0''.26$. It is in the direction of the center of the galaxy IC 4765-f01-1504 (Carrasco et al. 2006). This source has negligible emis-

¹ Institut de Recherche en Astrophysique et Planétologie, 9, av du Colonel Roche, BP 44346, 31028 Toulouse Cedex 4, France, email: Dacheng.Lin@cesr.fr

² Gemini Observatory/AURA, Southern Operations Center, Casilla 603, La Serena, Chile

³ Department of Astronomy and Astrophysics, Pennsylvania State University, 525 Davey Lab, University Park, PA 16802, USA

⁴ Sydney Institute for Astronomy (SfA), School of Physics, The University of Sydney, NSW 2006, Australia

sion above 2 keV. We describe the multi-wavelength observations of the source and the data reduction in Section 2. In Section 3, we first give the multi-wavelength detections of the source, followed by presentations of its detailed X-ray spectral and timing properties. We discuss its possible nature in Section 4 and draw our conclusions in Section 5.

2. DATA ANALYSIS

2.1. *XMM-Newton* Observations

2XMMi J184725.1-631724 was observed twice by *XMM-Newton* (Table 1), on 2006 September 7 and 2007 April 16. These two observations of this source will be referred to hereafter as XMM1 and XMM2, respectively. The source was detected in all the three European Photon Imaging Cameras in the imaging mode, i.e., pn, MOS1, and MOS2 (Jansen et al. 2001; Strüder et al. 2001; Turner et al. 2001), in both observations. The source was also detected by the Optical Monitor (OM; Mason et al. 2001) in XMM1, but it was not in the FOV of the OM in XMM2. In XMM1, the two UV filters UVW1 and UVM2 were used, and we obtained the source detection information directly from the pipeline products.

We used SAS 10.0.0 and the calibration files of 2010 November for reprocessing the X-ray event files and follow-up analysis. The data in strong background flare intervals, mostly at the end of the XMM2 observation in the pn camera, are excluded following the SAS thread for the filtering against high backgrounds. The final exposures used are given in Table 1. We extracted the source spectra of the pn, MOS1, and MOS2 cameras from a circular region centered on the source using 15'' and 35'' radii for XMM1 and XMM2, respectively. A smaller radius was used for XMM1 because the source was fainter and near the CCD gap. The background spectrum was extracted from a large circular region with a radius of 100'' near the source in each camera. The event selection criteria followed the default values in the pipeline (see Table 5 in Watson et al. (2009)). We rebinned the spectra to have at least 20 counts in each bin so as to adopt the χ^2 statistic for the spectral fits.

We also extracted light curves from the pn camera, which has a larger effective area and a higher timing resolution than the MOS cameras, using the same apertures as those for spectral extraction. We first extracted background-subtracted light curves with a bin size of 250 s, using the SAS task *epiclccorr* to apply relative corrections. To create the power density spectra (PDS), we also extracted light curves from the source region using the frame time as the bin size, which is 199.1 ms for XMM1 (using the extended-full-frame mode) and 73.4 ms for XMM2 (using the full-frame mode). Considering that the source is very soft and the background dominates above 2 keV, all light curves were extracted in the energy range 0.2–2.0 keV. We calculated the PDS using a similar procedure as, e.g., Goad et al. (2006). The XMM1 199.1 ms and XMM2 73.4 ms pn light curves were split into segments each with 32768 and 65536 data bins, respectively, resulting in four segments for XMM1 and five for XMM2. The PDS was calculated for each segment, and all PDS for each light curve were merged and averaged by binning in frequency using a logarithmic fac-

tor of 1.1, under the condition that each bin contains at least 20 individual PDS measurements. The errors were calculated from the sample standard deviation of PDS measurements in each bin.

2.2. *ROSAT* and *Swift* Observations

Our source was not detected in the *ROSAT* All-Sky Survey in 1990, which had a detection limit of 0.1–2.4 keV flux 5×10^{-13} erg s $^{-1}$ cm $^{-2}$ (Voges et al. 1999). Our source was in the FOV of one *ROSAT* PSPC pointed observation (the sequence number 800256, 1992 October, ~ 11 ks), at an off-axis angle of $\sim 2.6'$. It was not detected either and was (thus) not listed in the WGA catalog of the *ROSAT* point sources (White et al. 1994). We calculated the confidence interval of the source detection using Bayesian statistics as described in Kraft et al. (1991). Circular source and background regions with radii of 40'' and 2' respectively were used. The corresponding (ancillary plus photon redistribution) response matrix was generated and used to convert the count rates to the fluxes.

At our request, the *Swift* Gamma Ray Burst Explorer mission (Gehrels et al. 2004) observed the field of 2XMMi J184725.1-631724 on 2011 February 23 for a total of 5 ks (observation ID 00031930001). The X-ray telescope (XRT; Burrows et al. 2005) was operated in Photon Counting mode (Hill et al. 2004). X-ray data were reduced with the task *xrtpipeline* version 0.12.1. We found an enhanced count rate at the position of our source, but it is very weak. We also calculated the confidence interval of the detection. Radii of 23''5 and 235'' were used for the circular source and background regions, respectively. The corresponding response matrix was generated using the calibration files of 2011 February. The UV-Optical Telescope (UVOT; Roming et al. 2005) was operated using the UVW1 filter for 5 ks. The magnitude and flux were measured with the task *uvotsource* version 3 based on the most recent UVOT calibration as described in Poole et al. (2008) and Breeveld et al. (2010). Circular source and background regions with radii of 5'' and 20'', respectively, were used.

2.3. *Optical* Observations

Our source is in the direction of the center of the galaxy IC 4765-f01-1504 (Carrasco et al. 2006). This galaxy is located in the background of the rich group of galaxies IC 4765 (also known as Abell S0805, $z=0.01497$). It was imaged with the 1.3 m Warsaw telescope at Las Campanas Observatory in Chile through the standard Johnson V and Cousins I filters in 1998. We used the V- and I-filter images from Carrasco et al. (2006) to derive the main photometric parameters of the galaxy with a Sérsic model in GALFIT (Peng et al. 2010). The images have a FWHM of the PSF of about 1''.2.

Carrasco et al. (2006) also obtained an optical spectrum of the galaxy on 1999 June 19 with the Wide Field CCD camera mounted on the 2.5 m Du Pont Telescope at the Las Campanas Observatory in Chile, but it has poor quality. We obtained a new longslit spectrum of this galaxy with the Gemini Multi-Object Spectrograph (GMOS, Hook et al. 2004) at the Gemini South Telescope in the queue mode. The observation was made on the night of 2011 March 19 (UT) during bright time (illumination fraction 0.99), under photometric conditions

TABLE 1
XMM-Newton OBSERVATION LOG

Observation ID	Date	off-axis angles (arcmin) pn/MOS1/MOS2	Duration (ks)	Exposure(ks) pn/MOS1/MOS2	Filter
0405550401(XMM1)	2006-09-06.98	3.9/3.0/3.7	28.0	19.5/27.6/27.6	medium
0405380501(XMM2)	2007-04-16.31	9.0/8.5/9.4	34.7	20.5/32.2/31.9	thin1

and $\sim 1''$ seeing. The 400 lines/mm ruling density grating (R400) centered at 5500\AA was used, to minimize the effect of moon illumination. The slit width was set to $1''$. A total of four exposures of 900 s each were obtained. Small offsets in the spectral direction (50\AA) towards the blue and the red were applied between exposures to allow for the gaps between CCDs and to avoid any loss of important lines present in the spectra. Spectroscopic flats and comparison lamp (CuAr) spectra were taken after each science exposure. In addition, the spectrophotometric standard star LTT 7379 was observed at the end of the night to flux calibrate the science spectrum.

The observations were processed with the Gemini IRAF package version 1.9 in IRAF. All science exposures, comparison lamps and spectroscopic flats were bias subtracted and trimmed. Spectroscopic flats were processed by removing the calibration unit plus GMOS spectral response and the calibration unit uneven illumination, normalizing and leaving only the pixel-to-pixel variations and the fringing. The resulting two-dimensional spectra were then wavelength calibrated, corrected by S-shape distortions, sky-subtracted, extracted to a one-dimensional format using a fixed aperture of $7''.8$ in diameter, and then average combined. The final spectrum has a resolution of $\sim 8.8\text{\AA}$ (FWHM) and a dispersion of $\sim 1.36\text{\AA pixel}^{-1}$, covering a wavelength interval of $\sim 4000\text{--}7600\text{\AA}$. The signal-to-noise ratio is about 40 at 5500\AA .

We measured the redshift of the galaxy with two methods. In the first method, we cross-correlated the spectrum with a high signal-to-noise template using the *fxcor* routine in the IRAF RV package. The error was estimated using the R statistic of Tonry & Davis (1979): $\sigma_v = (3/8)(w/(1+R))$, where w is the FWHM of the correlation peak and R is the ratio of the correlation peak height to the amplitude of the antisymmetric noise. In the second method, we identified the most prominent absorption lines (as no clear emission lines were detected) in the spectrum and derived the redshift by employing a line-by-line Gaussian fit using the *rvidline* routine in the IRAF RV package.

3. RESULTS

3.1. The Source and the Multi-wavelength Observations

2XMMi J184725.1-631724 was detected in X-rays in both XMM1 and XMM2. We see no clear X-ray emission of our source from the *ROSAT* observation in 1992 October and the *Swift* observation in 2011 February, indicating variability factors of >64 and >12 , respectively, compared with XMM2 (the 0.2–10 keV absorbed flux; see Section 3.4). Here we concentrate on observations in other wavelengths.

The source position from the 2XMM catalog has been astrometrically corrected by matching with the optical catalog USNO B1.0 (Monet et al. 2003). For XMM1 and

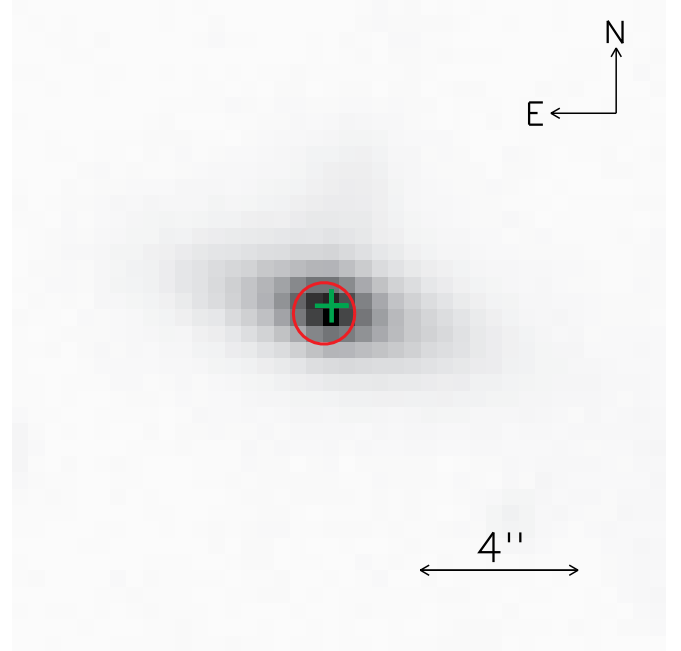


FIG. 1.— The optical image of the galaxy in the V band. The pixel size is $0''.414$. The green plus marks the central position of the galaxy obtained from the fits to its V- and I-band profiles using a Sérsic model, and it is at RA=18:47:25.14, Dec=−63:17:24.77 (J2000). The red circle is centered at the X-ray position, with the radius corresponding to the $3\text{-}\sigma$ error.

XMM2, a very small correction was invoked (a fraction of an arcsec). We compared the corrected positions of ten of the brightest X-ray sources in each observation with the positions of optical counterparts from the USNO B1.0 catalog and found that most of the offsets between the matches are less than $0.5''$, indicating successful astrometric corrections.

Table 2 gives the detection of a UV source in UVW1 and UVW2 from the XMM1 OM at a position within the $2\text{-}\sigma$ positional error from 2XMMi J184725.1-631724 and is probably its UV counterpart. There is also a UV source detected near our source in UVW1 from the *Swift* UVOT. After applying the astrometric correction using the USNO-B1.0 catalog with the XMM-Newton SAS task *eposcorr*, we obtain its position of RA=18:47:25.14 and Dec=−63:17:25.04 (J2000), within the $1\text{-}\sigma$ error from the X-ray position. Its magnitude and flux are 18.67 ± 0.04 and $(1.34 \pm 0.05) \times 10^{-16} \text{ erg s}^{-1} \text{ cm}^{-2} \text{\AA}^{-1}$, respectively. We note that the UV filter set in the UVOT is different from that of the XMM-Newton OM, and the above values should not be directly compared with the OM measurements in XMM1 above. Grupe et al. (2008a) measured an offset between the magnitudes from the two instruments of $W1_{\text{OM}} - W1_{\text{UVOT}} = 0.78$ by comparing several field stars in the images of the AGN Mkn 335. With this taken into account, there seems to be little variability in the UV between the two epochs.

TABLE 2
THE COUNTERPART CANDIDATES IN UV, OPTICAL, AND IR

UV (XMM1 OM)			Optical (USNO B1.0)				IR (2MASS PSC)			
r	UVW1	UVM2	r	B2	R2	I	r	J	H	K
(arcsec)	(AB mag/flux(10^{-16} erg s $^{-1}$ cm $^{-2}$ Å $^{-1}$))		(arcsec)		(mag)		(arcsec)		(mag)	
0.52	19.65 \pm 0.10/1.78 \pm 0.17	19.83 \pm 0.19/2.38 \pm 0.41	0.16	16.1	15.33	15.40	0.31	15.29 \pm 0.07	14.59 \pm 0.09	14.30 \pm 0.08

NOTE. — The r columns are the offsets of the counterparts from 2XMMi J184725.1-631724. The magnitudes/fluxes are not corrected for the Galactic reddening.

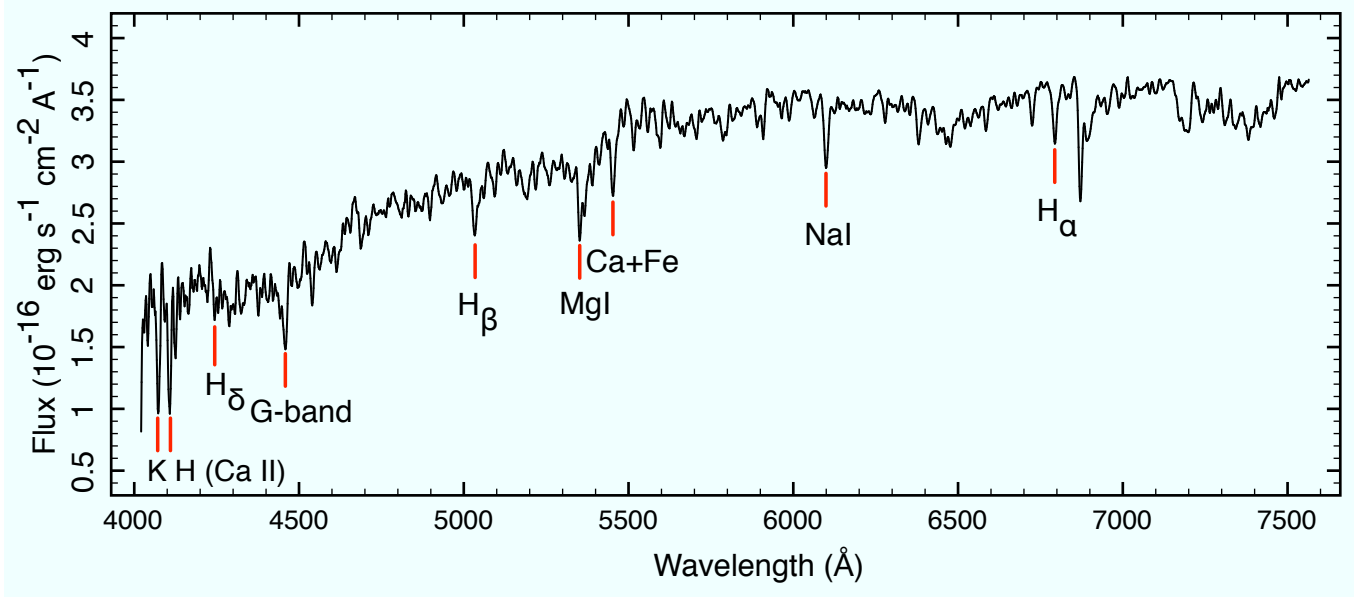


FIG. 2.— The smoothed spectrum of the galaxy IC 4765-f01-1504 from the Gemini South Telescope, with the most important absorption lines identified. The drop at 6870 Å is due to the atmosphere OH absorption.

The optical and IR counterpart candidates of the source from the USNO B1.0 and 2MASS Point Source Catalogs are given in Table 2. The optical counterpart, the galaxy IC 4765-f01-1504, is shown in Figure 1 (Carrasco et al. 2006). Our fits of the V- and I-band images using a Sérsic model give integrated magnitudes of 16.99 ± 0.01 and 15.62 ± 0.02 , effective radii of $2''.52 \pm 0''.04$ and $2''.94 \pm 0''.09$, Sérsic indices of 3.54 ± 0.06 and 4.14 ± 0.13 , and apparent axis ratios of 0.238 ± 0.003 and 0.271 ± 0.003 , respectively. This galaxy may be an elliptical galaxy, which typically has a Sérsic index of 4. The axis ratios above would imply a high inclination of this galaxy if its intrinsic ellipticity is low.

Figure 2 shows the spectrum of IC 4765-f01-1504 from the Gemini South Telescope. No clear emission lines were detected, supporting the identification as an elliptical galaxy. A redshift of $z=0.0353 \pm 0.0001$ was obtained from both the cross-correlation method, with $R = 12.80$, and the absorption line fit method, indicating a perfect agreement between them. This redshift disagrees with the value of 0.0869 obtained by Carrasco et al. (2006), which used the cross-correlation method (as there were no significant emission lines detected). Considering that our new spectrum has much better quality, we adopt this new redshift. We measured a $3\text{-}\sigma$ upper limit of [OIII] 5007 Å of 0.9×10^{-15} erg s $^{-1}$ cm $^{-2}$. Assuming a flat universe with the Hubble constant $H_0=73$ km s $^{-1}$ Mpc $^{-1}$ and the matter density $\Omega_M=0.27$, this redshift corre-

sponds to a comoving radial distance of 143.9 Mpc and a luminosity distance of 149.0 Mpc, which will be used in this paper. The absolute V and K magnitudes of this galaxy are -19.2 and -21.6, respectively, after the Galactic extinction correction (Schlegel et al. 1998). Based on the BH mass vs. bulge luminosity relations from Graham (2007), Lauer et al. (2007) and Marconi & Hunt (2003), the above magnitudes imply the mass of the SMBH in IC 4765-f01-1504 to be about 10^7 and $10^6 M_\odot$ if the bulge/total luminosity ratio is 1 or 0.1, respectively. Because the sample of galaxies in the above studies were generally brighter than IC 4765-f01-1504 and these relations have large intrinsic scattering, these mass estimates might have an uncertainty as large as one order of magnitude.

3.2. X-ray Spectral Modeling

We fitted the spectra of 2XMMi J184725.1-631724 from both XMM1 and XMM2 using various spectral models. We jointly fitted the spectra from all three cameras, i.e., pn, MOS1, and MOS2, and their relative normalizations were left free. We only report the normalization results corresponding to the pn camera. MOS1 and MOS2 differ by about 10% (the largest one $\sim 20\%$), less than the error bars. We fitted the spectra in the 0.2–10 keV energy band.

We were unsure the X-ray emission mechanism of our source. Thus we first tested the common single-component models to see whether any of them can de-

TABLE 3
SPECTRAL MODELING RESULTS

Model	Obs	N_H (10^{20} cm $^{-2}$)	$kT_{\text{MCD/BB}}$ (eV)	$N_{\text{MCD/BB}}$ (10^4)	$\Gamma_{\text{PL/SIMPL}}$	$N_{\text{PL}}/f_{\text{SC}}$ ($10^{-5}/\%$)	$\chi^2_\nu(\nu)$	$f_{\text{MCD/BB}}$ (%)	F_{abs} (10^{-12} erg s $^{-1}$ cm $^{-2}$)	F_{unabs} (10^{-12} erg s $^{-1}$ cm $^{-2}$)	L (10^{43} erg s $^{-1}$)
MCD+PL	XMM1	8.6 ± 0.5	65.8 ± 5.0	$1.56^{+1.21}_{-0.63}$	3.72 ± 0.62	1.79 ± 0.32	0.92(115)	$84.5^{+7.3}_{-14.8}$	0.22 ± 0.01	1.76 ± 0.19	1.70 ± 0.44
	XMM2		93.1 ± 2.2	$1.45^{+0.34}_{-0.23}$	3.27 ± 0.70	3.75 ± 1.39	1.20(284)	$96.4^{+1.9}_{-6.1}$	1.93 ± 0.03	$10.18^{+1.00}_{-0.57}$	6.38 ± 0.66
SIMPL(MCD)	XMM1	8.5 ± 0.5	65.1 ± 5.5	$1.73^{+1.65}_{-0.73}$	3.71 ± 0.63	$3.33^{+3.98}_{-1.69}$	0.92(115)	$90.0^{+3.7}_{-7.1}$	0.22 ± 0.01	$1.75^{+0.35}_{-0.24}$	1.81 ± 0.57
	XMM2		92.9 ± 2.4	1.49 ± 0.32	3.33 ± 0.78	$0.83^{+1.32}_{-0.49}$	1.20(284)	$97.7^{+0.9}_{-2.2}$	1.92 ± 0.03	10.21 ± 0.89	6.40 ± 0.72
BB+PL	XMM1	7.4 ± 0.7	57.8 ± 3.9	$1.63^{+1.13}_{-0.56}$	3.71 ± 0.59	1.76 ± 0.28	0.92(115)	$78.2^{+9.5}_{-17.2}$	0.22 ± 0.01	1.23 ± 0.11	0.59 ± 0.14
	XMM2		78.2 ± 1.6	2.37 ± 0.41	3.89 ± 0.61	5.54 ± 1.46	1.18(284)	$86.0^{+7.6}_{-14.4}$	1.92 ± 0.03	$7.59^{+1.15}_{-0.51}$	2.79 ± 0.39
SIMPL(BB)	XMM1	7.2 ± 0.5	57.7 ± 4.1	$1.81^{+1.3}_{-0.65}$	3.71 ± 0.59	$5.48^{+4.81}_{-2.31}$	0.92(115)	$87.8^{+3.9}_{-7.1}$	0.22 ± 0.01	1.18 ± 0.18	0.59 ± 0.15
	XMM2		77.5 ± 2.2	$2.58^{+0.71}_{-0.45}$	4.25 ± 0.83	$3.35^{+3.56}_{-1.63}$	1.18(284)	$94.2^{+2.4}_{-4.6}$	1.92 ± 0.03	7.2 ± 0.68	2.70 ± 0.31

NOTE. — The column $f_{\text{MCD/BB}}$ refers to the unabsorbed flux fraction of the MCD/BB component in the 0.2–10 keV energy band (for the models SIMPL(MCD) and SIMPL(BB), it refers to the unscattered part). F_{abs} and F_{unabs} are the total absorbed and unabsorbed fluxes in the 0.2–10 keV energy band, respectively. The luminosity L was calculated using the unabsorbed bolometric flux of each spectral component (the PL component was integrated down to 0.2 keV). All errors are at a 90%-confidence level.

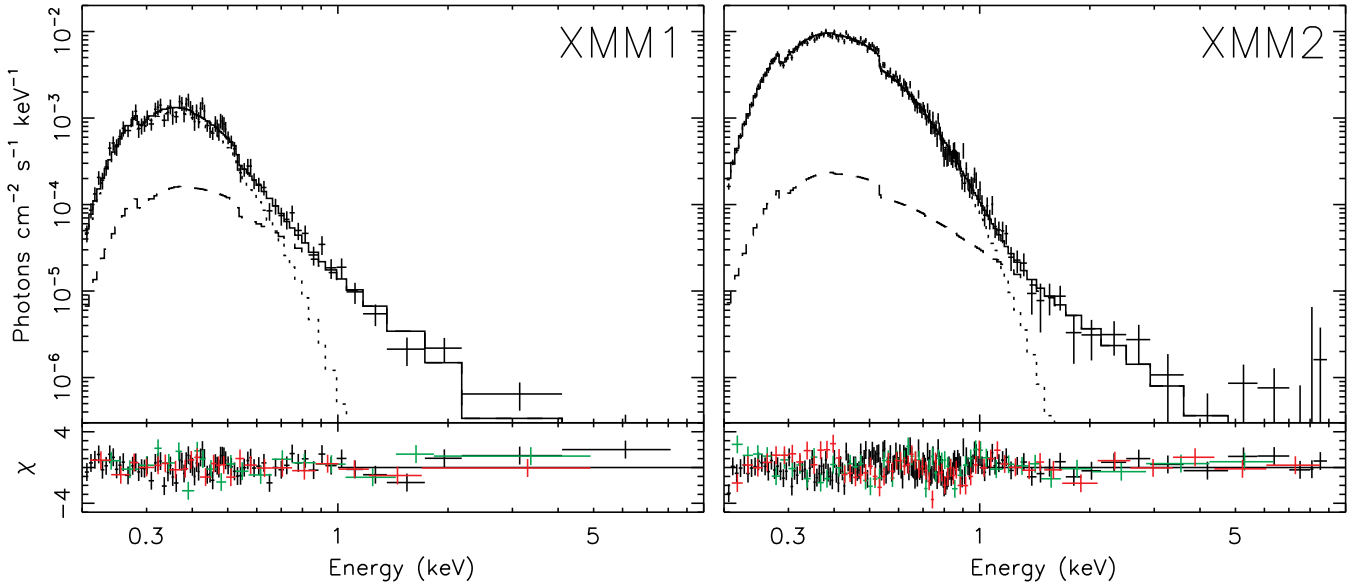


FIG. 3.— The unfolded spectra and the fit residuals using the model MCD+PL. For clarity, only the pn spectra are shown for the unfolded spectra. The dotted, dashed, and solid lines are for the MCD and PL components and the total model, respectively. The residuals are shown for all three cameras (black/red/green for pn/MOS1/MOS2, respectively).

scribe our X-ray spectra well: a single temperature blackbody (BB), a multi-color disk (MCD), a PL, a broken PL, a cut-off PL, an APEC thermal plasma model, and a thermal bremsstrahlung spectrum. They are models bbodyrad, diskbb, powerlaw, bknpower, cutoffpl, APEC, and brems in XSPEC, respectively. All models include the absorption described by the WABS model in XSPEC; our results change little with alternative absorption models such as PHABS or TBABS in XSPEC. All these simple models fail to describe one or both of the *XMM-Newton* spectra, with residuals above 1 keV typically seen. For indication, we report the PL index Γ_{PL} of the fits using the PL model. We obtained $\Gamma_{\text{PL}} = 5.86 \pm 0.27$ for XMM1 ($\chi^2_\nu(\nu)=1.13(117)$) and 6.88 ± 0.09 for XMM2 ($\chi^2_\nu(\nu)=2.25(286)$). The lower χ^2 value for XMM1 to some degree is due to poorer data.

We next attempted to fit the spectra with the double-component models MCD+PL and BB+PL, finding that they describe both the XMM1 and XMM2 spectra much better than the above common single-component models, with the χ^2 values decreased by more than 140

for the total degrees of freedom of about 400 of both the XMM1 and XMM2 spectra. As a way to model the hard component self-consistently, we also fitted the spectra with SIMPL(MCD) and SIMPL(BB). SIMPL (in XSPEC12; Steiner et al. 2009) is an empirical convolution model of Comptonization in which a fraction (f_{SC}) of the input seed photons are converted into a power law parametrized by an index (Γ_{SIMPL}). We assume that all the scattered photons are up-scattered in energy in this model.

The best-fitting values of the column density are consistent between XMM1 and XMM2, with $N_H = (7.6^{+1.5}_{-2.6})$ and $(8.6 \pm 0.6) \times 10^{20}$ cm $^{-2}$, respectively, using the model MCD+PL. Thus, we chose to fit both spectra with a common value of N_H . The final results are given in Table 3. The best-fitting values of N_H are slightly higher than the Galactic value of 6.1×10^{20} cm $^{-2}$ from the Leiden/Argentine/Bonn Survey of Galactic HI (Kalberla et al. 2005), probably indicating a small intrinsic absorption.

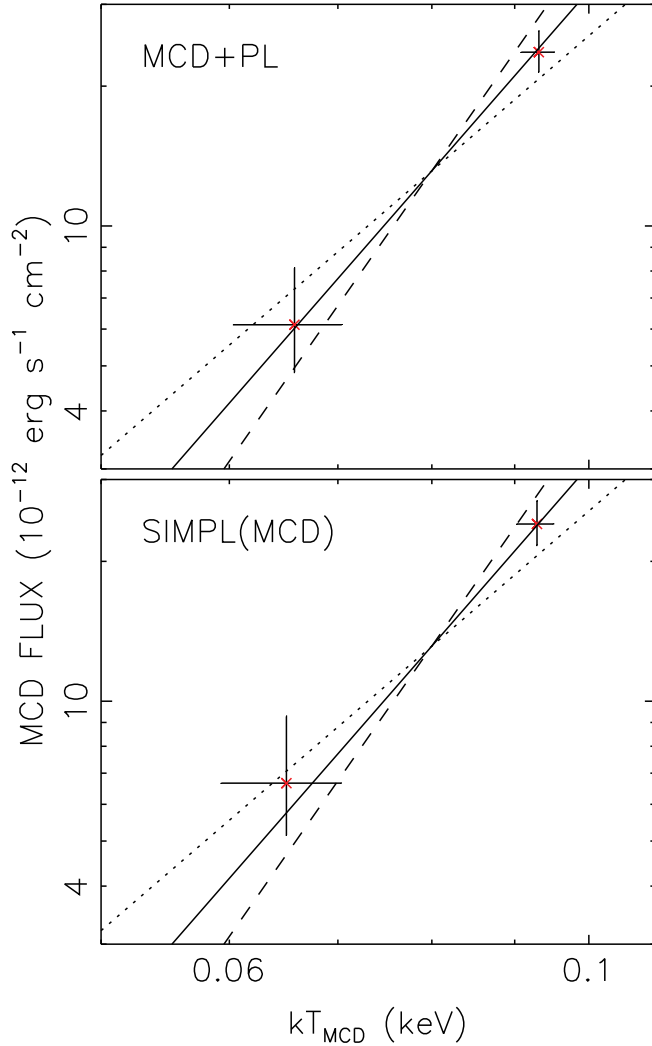


FIG. 4.— The MCD flux versus kT_{MCD} using the models MCD+PL and SIMPL(MCD). The solid, dotted, and dashed lines plot the $L \propto T^4$, $L \propto T^3$, and $L \propto T^5$ relations, as a guidance.

For the model MCD+PL, we show the unfolded spectra and residuals in Figure 3. In this model, the spectra are dominated by the MCD component at energies below 1 keV. The fraction of the MCD component is about 84.5% and 96.4% for XMM1 and XMM2, respectively (the 0.2–10 keV unabsorbed flux; Table 3). The 0.2–10 keV flux increases from XMM1 to XMM2 by a factor of 8.8 (absorbed) or 5.8 (unabsorbed). We also estimate the luminosity, using the bolometric flux of each spectral component. The disk inclination is uncertain, and we assume it to be 60° . The PL component diverges at low energies, and we integrate its flux above 0.2 keV. We obtain luminosities of 1.70 and $6.38 \times 10^{43} \text{ erg s}^{-1}$ for XMM1 and XMM2, respectively (Table 3). For comparison, the corresponding 0.2–10 keV luminosities are 0.47 and $2.70 \times 10^{43} \text{ erg s}^{-1}$, respectively.

We plot the MCD bolometric flux versus its temperature at the inner disk radius kT_{MCD} in Figure 4 (the upper panel). We can see that the evolution of the MCD luminosity is consistent with the $L \propto T^4$ track (the solid line), which implies a constant inner disk radius with the change in luminosity. We note that this is based on the

only two observations available. The disk temperature is relatively low, only $kT_{\text{MCD}} = 65.8$ and 93.1 eV for XMM1 and XMM2, respectively. The PL component is weak, and its parameter values have relatively large uncertainties. Its index is consistent between XMM1 and XMM2 and is relatively steep, with Γ_{PL} about 3.5. Forcing XMM1 and XMM2 to have the same value of Γ_{PL} in the fit, we see a change of the PL normalization N_{PL} by a factor of 2.6 (4.5σ).

The model SIMPL(MCD) gives results very similar to the model MCD+PL (Table 3 and Figure 4), in terms of the MCD temperature, the thermal fraction, etc. It infers that only about $f_{\text{SC}}=3\%$ and 1% of the thermal disk emission is Comptonized to the hard emission in XMM1 and XMM2, respectively. This model, with a natural cut-off at low energies for the hard component, infers luminosities similar to those of the model MCD+PL obtained by integrating the PL flux down to 0.2 keV (Table 3).

The spectra can also be fitted almost equally well using the models BB+PL and SIMPL(BB) (Table 3). The BB component dominates in both XMM1 and XMM2, contributing $\gtrsim 80\%$ of the 0.2–10 keV flux, similar to the MCD component in the models MCD+PL and SIMPL(MCD). Its effective temperature kT_{BB} is also low, about 58 and 78 eV for XMM1 and XMM2, respectively. The MCD and BB models have very similar spectral shapes at high energies (Makishima et al. 1986), but their differences become large at low energies. We estimate their differences in the UV. We have measurements from two UV filters, i.e., UVW1 and UVM2, from XMM1. The flux densities of the MCD component in the model MCD+PL from XMM1 are (2.15 ± 0.69) and $(3.68 \pm 1.18) \times 10^{-17} \text{ erg s}^{-1} \text{ cm}^{-2} \text{ \AA}^{-1}$ at the effective wavelengths of UVW1 (2910 Å) and UVM2 (2310 Å), respectively. The corresponding values for the BB component in the model BB+PL from XMM1 are (0.40 ± 0.16) and $(1.00 \pm 0.40) \times 10^{-19} \text{ erg s}^{-1} \text{ cm}^{-2} \text{ \AA}^{-1}$, respectively. The corresponding flux densities measured with UVW1 and UVW2 are (3.00 ± 0.47) and $(5.08 \pm 1.45) \times 10^{-16} \text{ erg s}^{-1} \text{ cm}^{-2} \text{ \AA}^{-1}$, respectively, after the Galactic dust extinction correction using a reddening value of $E(B-V) = 0.098$ (Schlegel et al. 1998) and assuming a spectral shape of a MCD model at low frequencies (i.e., a power law with a photon index of $2/3$). We see that the UV flux from the OM detection is much higher than the BB flux in the UV. It is closer to the MCD flux in the UV, but still there is about an order of magnitude difference, which will be discussed in Section 4. The flux of the PL component in the UV is hard to assess as this model is too steep and diverges at low energies (more than two orders of magnitude higher than that measured by the OM) and must be cut off below some energy. The models SIMPL(MCD) and SIMPL(BB) show no such problem, and their fluxes in the UV, from the whole model or only from the thermal components, are very close to the MCD and BB fluxes in the UV obtained above.

3.3. Fast X-ray Variability

The left panels of Figure 5 show the pn 250 s background-subtracted light curves. The background is at a level of about 3% and 2% for XMM1 and XMM2, respectively. The variations of the source count rate can

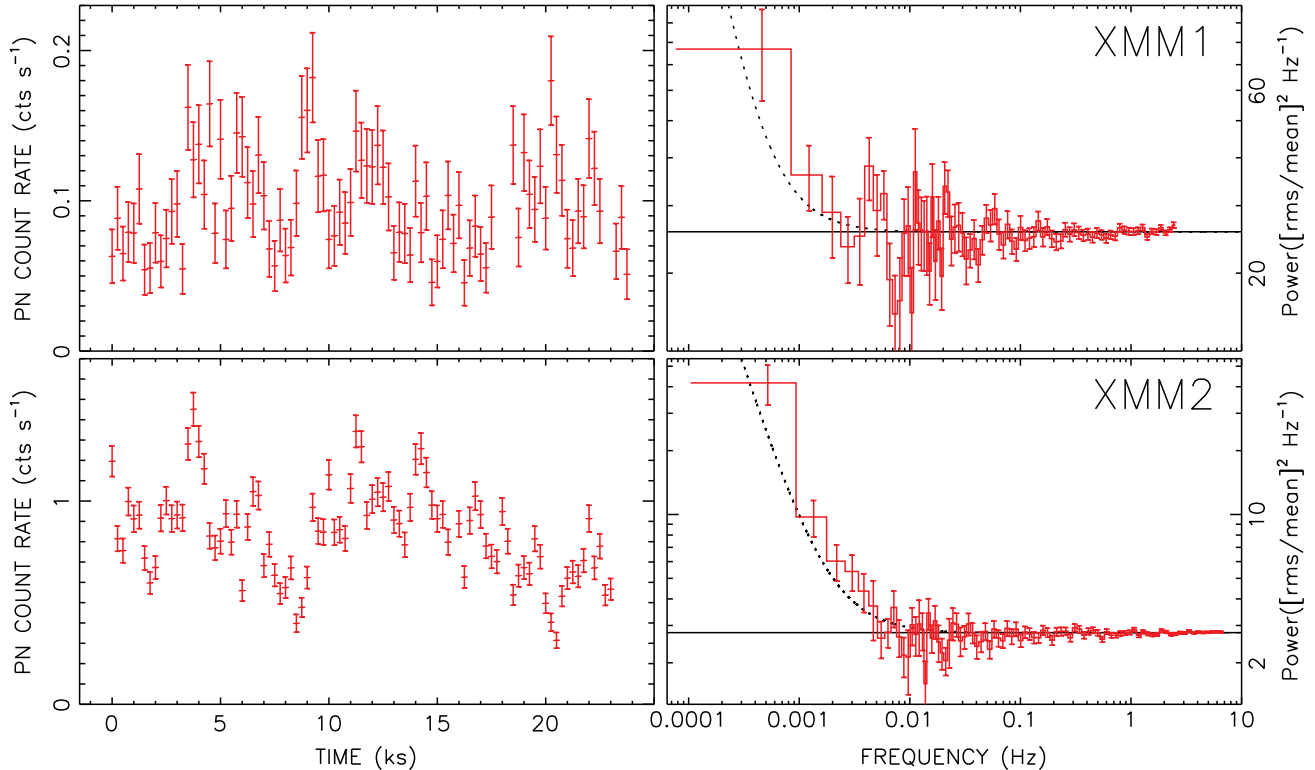


FIG. 5.— Left panels: The pn 250 s 0.2–2.0 keV background-subtracted light curves binned at 199.1 ms for XMM1 and 73.4 ms for XMM2. The right panels: The PDS of the pn 0.2–2.0 keV light curves. The black solid constant line is the average PDS above 0.1 Hz, representing the Poisson level, and the dotted line is the best-fitting model of a PL plus a constant.

TABLE 4
THE FIT RESULTS OF THE PDS USING A PL PLUS A CONSTANT.

Obs	Γ_{PL}	$N_{\text{PL}} (10^{-5})$	C_{P}	$\chi^2_{\nu}(\nu)$	rms(%)
XMM1	$1.74^{+1.13}_{-0.57}$	$3.49^{+27.70}_{-3.48}$	25.59 ± 0.17	1.07(75)	21.2 ± 5.3
XMM2	1.65 ± 0.19	$8.17^{+20.42}_{-6.75}$	2.77 ± 0.01	1.06(82)	21.1 ± 1.9

NOTE. — The column rms refers to 0.0001–0.01 Hz fractional rms after subtracting the Poisson level. N_{PL} is the PL normalization at 1 Hz. All errors are at a 90%-confidence level, except for the rms, whose 1- σ errors are given.

be clearly seen for both observations. For XMM2, which has higher count rates, we see that the source varies by a factor of ~ 4 within 5 ks.

The right panels of Figure 5 show the pn PDS of XMM1 and XMM2. Both PDS are flat at frequencies above 0.1 Hz, representing the Poisson level. Their averages above 0.1 Hz weighted by the errors differ from the expected Poisson noise values by $<0.3\%$. Below 0.01 Hz, both PDS show a clear deviation from the Poisson level (the black solid line). We successfully fitted both PDS with a power-law (PL) plus a constant C_{P} , accounting for the Poisson level, and the results are given in Table 4. The PL index Γ_{PL} is about 1.7 for both observations. We evaluate the fractional rms within 0.0001 to 0.01 Hz after subtracting the Poisson level and obtain a value of $(21.2 \pm 5.3)\%$ and $(21.1 \pm 1.9)\%$ for XMM1 and XMM2, respectively. The above results indicate that the source shows similar variability in both XMM1 and XMM2.

The large fast variability seen above should be due to the thermal component from the models in Table 3, as the hard component is very weak (e.g., $<4\%$ in XMM2, in terms of the 0.2–2.0 keV pn count rates). To see the

cause of the variability, we extracted the high- and low-state spectra from the bright observation XMM2, corresponding to intervals with the pn count rate higher or lower than $0.8 \text{ counts s}^{-1}$, respectively (Figure 5). We fitted these two spectra simultaneously using the model SIMPL(MCD) with a common value of N_{H} . We find that the MCD temperature in the low state is smaller than in the high state by 10 eV at a $4.4\text{-}\sigma$ confidence level. Their MCD normalizations are consistent with being the same within the error bars. The parameters of the hard component have large uncertainties, making it hard to constrain any trend. Based on the MCD model, the above results provide one explanation of our large fast variability: it is caused by the fast variations in the mass accretion rate, with the disk truncated at a constant radius.

3.4. Comparison with *ROSAT* and *Swift* Observations

We obtain count rates of $<1.9 \times 10^{-3}$ and $1.3^{+2.4}_{-0.3} \times 10^{-3} \text{ counts s}^{-1}$ for the *ROSAT* PSPC observation in 1992 October and the *Swift* XRT observation in 2011 February, respectively. The $3\text{-}\sigma$ upper bounds are given above, and the lower bounds are zero. Using the response matrices corresponding to the source extraction regions used and the fit results of the model SIMPL(MCD) for XMM1, these count rates correspond to the 0.2–10 keV absorbed fluxes of <0.3 and $0.6^{+1.0}_{-0.3} \times 10^{-13} \text{ erg s}^{-1} \text{ cm}^{-2}$, respectively, and the 0.2–10 keV unabsorbed fluxes of <2.4 and $4.5^{+8.3}_{-2.4} \times 10^{-13} \text{ erg s}^{-1} \text{ cm}^{-2}$, respectively. Thus, the source varied by a factor of >64 and >43 between the *ROSAT* pointed observation in 1992 and XMM2, using the 0.2–10 keV absorbed and unabsorbed fluxes, respectively. The corresponding variation factors between

XMM2 and the *Swift* observation in 2011 are >12 and >8 , respectively.

4. DISCUSSION

4.1. The Nature and Implication of the Soft Component

The remarkable features of 2XMMi J184725.1-631724 are the extreme softness of its X-ray spectra and the large variability. Understanding the nature and implication of the soft component which dominates the X-ray spectra will help to pin down the nature of the source. As it is in the direction coincident with the center of the galaxy IC 4765-f01-1504, we first assume that its X-ray emission is associated with the SMBH in this galaxy. This can be due to either a tidal disruption event or an AGN.

The fits with the models MCD+PL and SIMPL(MCD) above assume that there was a thermal disk emission, whose luminosity fraction was inferred to be very high, $\sim 90\%$. The evolution of the MCD luminosity is consistent with $L \propto T^4$, though only two observations are available. These properties are very similar to the thermal state of BH X-ray binaries (Remillard & McClintock 2006), in which the accretion disk is believed to be truncated at the innermost stable circular orbit (ISCO). Thus we assume that the disk is also truncated at the ISCO during these two observations and roughly estimate the BH mass from the MCD normalization N_{MCD} . Using a distance of 143.9 Mpc and assuming a disk inclination of 60° , we infer the BH mass to be $\sim 3 \times 10^5 M_\odot$, neglecting factors such as the spin and the hardening effect. If we replace the MCD model with the more realistic accretion disk model around a Kerr black hole *kerrbb* (in XSPEC; Li et al. 2005) and explore the parameter spaces of the disk inclination $0-75^\circ$, the spin parameter a^* $0-1$, and the hardening factor $1-1.7$, we obtain a range of the BH mass of $(0.06-3.81) \times 10^6 M_\odot$. Assuming the BH mass to be $5 \times 10^5 M_\odot$, the source would be at about 0.3 and 1.0 Eddington luminosity in XMM1 and XMM2, respectively, common values seen in the thermal state of BH X-ray binaries (Done et al. 2007). We note that the light crossing time of the inner accretion disk around a BH with this mass is ~ 50 s, about the timescale on which the source begins to show strong variability (Figure 5). The above mass estimate is consistent with that using the BH mass vs. bulge luminosity relations (Section 3.1), considering the large uncertainties of both methods.

Some AGN can be very soft, showing strong soft excesses (Puchnarewicz et al. 1992). The soft excess refers to the excess of emission below ~ 2 keV with respect to the extrapolation of the power-law fit of the continuum above 2 keV and is commonly observed in type-I AGN (Turner & Pounds 1989). The strongest soft X-ray excesses and variability are found in Narrow Line Seyfert 1 galaxies (NLS1s; e.g., Boller et al. 1996; Leighly 1999b,a; Grupe et al. 2010). The nature of the soft excess is still unclear. The above thermal disk model is one of the several competing models invoked (e.g., Walter & Fink 1993). The problem with this explanation is that the soft excesses from a sample of AGN with a large range of mass and luminosity have characteristic temperatures spanning a narrow range ($\sim 0.1-0.2$ keV), which is hard to explain (Gierliński & Done 2004; Crummy et al. 2006). The narrow range of the characteristic temperatures of the soft excesses finds a natural explanation if they are

due to atomic processes. There are two main scenarios, i.e., absorption and reflection. Gierliński & Done (2004) proposed the soft excess as an artifact of strong, relativistically smeared, partially ionized absorption. We test this model using the *swindl* model from XSPEC. We use the model *swindl*(PL), with Γ_{PL} required to be < 3.5 to make sure that it is not the steep PL describing the soft excess. We obtain the values of $\chi^2_\nu(\nu)$ to be 1.32(114) and 1.31(283) for XMM1 and XMM2, respectively. Both observations require strong velocities (> 0.5 and 0.29 ± 0.02 speed of light for XMM1 and XMM2, respectively) to smear the absorption/emission lines, which is hard to achieve from a radiatively driven accretion disk wind (Schurch & Done 2007; Schurch et al. 2009). The difference between XMM1 and XMM2 is mainly due to different absorption column densities and smearing velocities, requiring dramatic changes in the absorber.

In the reflection model, a series of soft X-ray emission lines below 2 keV, if strongly relativistically blurred, can produce the smooth soft excess feature. We follow Crummy et al. (2006) to use the model *kdblur*(PL+*reflionx*), where *kdblur* is the relativistic convolution and *reflionx* is a table model of the ionized reflection (see their references therein). In the fits we force XMM1 and XMM2 to have common values of N_{H} , the inclination, and the Fe abundance. We obtain $\chi^2_\nu(\nu) = 0.95(111)$ and $1.34(281)$ and reflection flux fractions ~ 0.94 and 1 (0.2–10 keV, unabsorbed) for XMM1 and XMM2, respectively. The fits require a low inclination ($17.1 \pm 7.6^\circ$), a high Fe abundance ($8.37^{+0.79}_{-2.65}$ solar value), and a steep illuminating power-law spectrum (reaching the upper index limit of 3.3 allowed in the model). The disk emissivity index is different between these two observations ($5.37^{+0.87}_{-0.27}$ and 8.99 ± 0.89 for XMM1 and XMM2 respectively), implying a very different disk structure. This model infers a highly spinning BH, with the inner disk radius at 2.38 ± 0.38 and $1.87^{+0.53}_{-0.19}$ gravitational radii for XMM1 and XMM2 respectively. Compared with the results from Crummy et al. (2006), the above values are extreme but not unique.

We see that both the absorption and reflection models invoke extreme environments to explain our source. The former requires absorbers at very high velocities and varying dramatically. The latter requires very steep illuminating spectra and very different disk emissivities between XMM1 and XMM2. In comparison, the thermal disk emission explanation for the soft component in our source is more reasonable. In this model, the difference between XMM1 and XMM2 is simply due to the change in the accretion rate. We note that the inferred inner disk temperatures are lower than the typical characteristic temperatures of the soft excesses in AGN, which might indicate that the soft component of our source has a different nature from soft excesses in AGN.

Our spectral fits did not combine both the UV and X-ray spectra. There is about one order of magnitude difference (about 9σ) between the UV fluxes of the thermal disk inferred from the soft X-ray spectral fits and the OM measurements (Section 3). This can be due to several factors. First, we have only used the simple MCD model, while a more realistic disk spectral model is probably needed to fit broadband data (about three decades in frequency here; Laor & Netzer 1989; Ross et al. 1992;

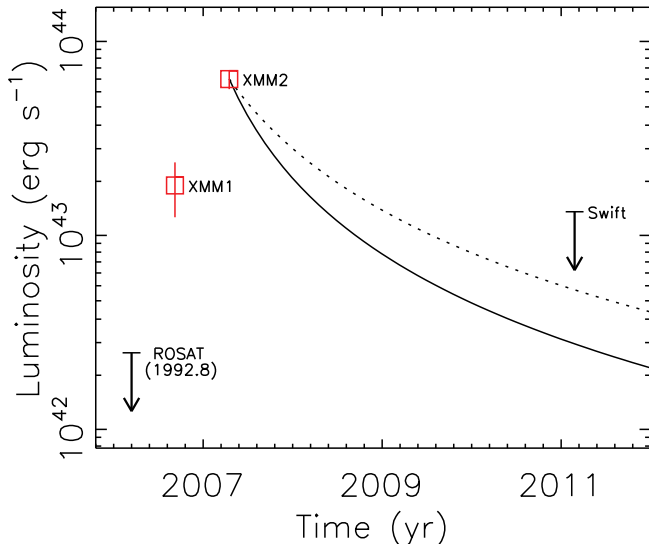


FIG. 6.— The long-term luminosity curve inferred from X-ray spectral fits. Arrows represent $3\text{-}\sigma$ upper bounds. Note that the *ROSAT* observation was made in 1992 October. The solid curve is $\text{Luminosity} = 3.45 \times 10^{43} [(\text{Time} - 2006.60\text{yr})/(1\text{yr})]^{-5/3} \text{ erg s}^{-1}$, and the dotted curve is $\text{Luminosity} = 7.57 \times 10^{43} [(\text{Time} - 2006.18\text{yr})/(1\text{yr})]^{-5/3} \text{ erg s}^{-1}$.

Vasudevan & Fabian 2009). Secondly, the starlight or hot gas emission might be significant in the UV. This is supported by the little variability of the UV emission between XMM1 and the *Swift* observation in 2011 February. Finally, some UV emission might come from the reprocessing of the X-ray emission in the outer disk or surrounding gas.

4.2. The Tidal Disruption Event Explanation

We show above that the X-ray emission in XMM1 and XMM2 can be best explained as coming from a thermal disk around a SMBH with a mass of $\sim 10^5\text{--}10^6 M_\odot$. The transient nature of the source makes it a great tidal disruption event candidate. This is further supported by the extreme softness of its X-ray spectra and the inactivity of the nucleus of the candidate host galaxy IC 4765-f01-1504. The inactivity of IC 4765-f01-1504, i.e., not an AGN, is indicated by its lack of significant optical emission lines (Figure 2). As our new optical spectrum was made four years after the flare, this also implies no detection of optical emission lines due to the flare at this stage. The 2MASS IR colors (Table 2) also put this galaxy in the region occupied by inactive galaxies in the color-color diagram (e.g., Hyland & Allen 1982). The estimated BH mass allows the tidal disruption of a solar-type star to be observable (Lidskii & Ozernoi 1979; Rees 1988). The luminosity reached $6.4 \times 10^{43} \text{ erg s}^{-1}$, which is about the average seen in other candidates (Komossa 2002; Esquej et al. 2007; Gezari et al. 2009). However, no previous candidates had soft X-ray spectra with such high quality during the peak of the flare to allow for the detailed spectral studies here.

One main feature of tidal disruption events is the temporal evolution. Such events are predicted to rise on timescales of several months and decay on timescales of months/years (Lidskii & Ozernoi 1979; Rees 1988, 1990). The decay approximately follows $L \propto (t - t_D)^{-5/3}$, where t_D is the tidal disruption time, for most candidates

(Maksym et al. 2010; Esquej et al. 2008; Halpern et al. 2004; Komossa & Bade 1999), consistent with the theory. XMM1 is fainter than XMM2, and they are separated by 211 days. If our source is due to tidal disruption, XMM1 should probably be in the rising phase, and XMM2 in the decay phase. We plot the luminosity curve in Figure 6. Two decay curves following $L \propto t^{-5/3}$ are also plotted, with XMM2 assumed to be in the decay. The dotted and solid curves assume t_D to be at half a year and one month before XMM1, respectively. These assumptions are reasonable, as the minimum period for the material to return to the SMBH (so as to accrete) after disruption is on the order of a month (Rees 1988; Evans & Kochanek 1989). These curves predict that the source luminosity in the *Swift* observation in 2011 February should be a factor of about 20 less than XMM2. Our detection limit is consistent with this. In the above, we concentrate only on the decay, as the connection from the rise to the decay is uncertain. The rise could probably take months, and there could be a short period of several months when the luminosity is maintained near the Eddington limit (Rees 1988, 1990). Future sensitive X-ray observations in the decay are needed to constrain the long-term evolution.

We see that our source showed large fast X-ray variability, with an rms of $\sim 21\%$ (Section 3.3) in both *XMM-Newton* observations. If they are really dominated by the thermal disk emission, the above rms value is high, compared with the values of $\lesssim 5\%$ typically seen in the thermal state of neutron-star (NS) or BH low-mass X-ray binaries (Lin et al. 2007; Remillard & McClintock 2006; McClintock & Remillard 2006). We note that our rms was integrated over two decades in frequency, the same as the above studies. Besides, in low-mass X-ray binaries, the power of the thermal disk typically scales with the frequency as ν^{-1} (McClintock & Remillard 2006), while the power for our source is steeper, scaling approximately as $\nu^{-1.7}$. Large fast variability and steep power can be seen sometimes in the thermal state of X-ray binaries, such as the flaring branch of bright NSs (Homan et al. 2002), which was ascribed to some local instability in the inner disk by Lin et al. (2009). For the case of our source, we have shown in Section 3.3 that its fast variability can be explained as due to fast variations in the mass accretion rate, which, in the context of a tidal disruption event, could reasonably be ascribed to shocks during drastic compression and distortion of the stellar material (Rees 1988). This does not occur in low-mass X-ray binaries, in which the mass is transferred through the Roche lobe. Thus we speculate that the large fast variability and the steep power in the thermal state is intrinsic to tidal disruption events. Among the previous tidal disruption event candidates with thermal X-ray peaks, the peak of NGC 5905 was the best observed. It showed an increase of a factor of ~ 3 during the peak, but it was over four days (Bade et al. 1996), and the data quality was not high enough to investigate the variability on much shorter timescales.

4.3. Comparison with AGN

2XMMi J184725.1-631724 is unlikely to be an AGN from the lack of bright optical emission lines. In the following we briefly compare the X-ray properties of our source with ultrasoft AGN to show their similarities and

differences. NLS1 galaxies typically show the steepest soft-X-ray spectra among AGN and have a typical photon index of around 3 (Boller et al. 1996; Grupe et al. 2010). The simple fits of the XMM1 and XMM2 spectra using the PL model indicate an extreme softness of our source that is not seen in NLS1s.

We estimate the optical-to-X-ray spectral slope α_{ox} using the flux densities in the rest frame of 2500 Å and 2 keV (Tananbaum et al. 1979). We obtain $\alpha_{\text{ox}} = 1.76 \pm 0.03$. The luminosity density in the rest frame of 2500 Å is $l_{2500} = (1.48 \pm 0.24) \times 10^{28} \text{ erg s}^{-1} \text{ Hz}^{-1}$. With this value of l_{2500} , the value of α_{ox} should be $\lesssim 1.3$, based on the sample of 92 Seyfert 1 galaxies in Grupe et al. (2010, their Figure 15). In fact 2XMMi J184725.1-631724 has about the highest value of α_{ox} and the lowest value of l_{2500} and is an outlier, compared with their sample. We note, however, the possible large uncertainty of α_{ox} for our source, whose star light contamination might be large, as discussed above.

There have been several ultrasoft AGN claimed in the literature. The NLS1 galaxy WPVS 007 has the softest X-ray spectrum among AGN detected during the *ROSAT* All-Sky Survey, with $\Gamma_{\text{PL}} \sim 8$ if fitted with a PL or $kT \sim 20$ eV with a BB (Grupe et al. 1995). It can be explained as emission from the inner disk (Grupe et al. 1995), but the quality of the data and the lack of simultaneous observations above 2.4 keV could make its soft excess due to the presence of a warm absorber (Grupe et al. 2008b). The narrow-line quasar PHL 1092 has *XMM-Newton* observations, and the X-ray spectra are steep ($\Gamma_{\text{PL}} \sim 4-5$), but the PL fit is not good when it is bright (Gallo et al. 2004; Miniutti et al. 2009). Its bright spectrum in 2003 was fitted with a model of MCD+PL plus an absorption line and a reflection component by Gallo et al. (2004); its soft excess was ascribed to the MCD component ($kT = 114 \pm 4$ eV), as in our study. The NLS1 galaxy 1H 0707-495 also shows an intense soft excess. Its X-ray spectra from *XMM-Newton* show $\Gamma_{\text{PL}} \sim 3.8$ (Boller et al. 2002). They were fitted with a model of BB+PL plus a reflection component by Fabian et al. (2009). From this model, both the thermal disk emission and the reflection contribute to the soft excess, but the latter dominates. We note that the above ultrasoft AGN show large short-term variability factors of a few and/or long-term variability factors of a few hundred, similar to our source. Thus the variability of our source is not extreme compared with NLS1s, but the softness of its X-ray spectra is hardly challenged. We note that the soft component in our source cools in low states, which is not generally seen in NLS1s (e.g., Miniutti et al. 2009).

4.4. Alternative Explanations

We explore the possibility that 2XMMi J184725.1-631724 is not associated with the SMBH in IC 4765-f01-1504. If it is an ultraluminous X-ray source (ULX) in this galaxy, it would have a luminosity about one order of magnitude brighter than the brightest ULX reported thus far, i.e., HLX-1 (Farrell et al. 2009). However, as derived above, both the spectral fits and the variability argument imply that this source most probably has a mass of $\sim 10^5 - 10^6 M_{\odot}$, and it should be within 0.5 kpc (3σ error) of the galaxy center. Being so massive and so close to the galaxy center, it seems unlikely to be a

source other than the central SMBH. Thus we deem that our source is not a ULX in IC 4765-f01-1504.

The other possibility is that 2XMMi J184725.1-631724 is a foreground Galactic source. Following Haakonsen & Rutledge (2009) and using the 0.2–10 keV absorbed flux of $1.92 \times 10^{-12} \text{ erg s}^{-1} \text{ cm}^{-2}$ (Table 3), we have the X-ray to IR flux ratio $f_{\text{X}}/f_{\text{J}} \sim 5$ for our source, making it unlikely to be a coronally active star. These stars generally have $f_{\text{X}}/f_{\text{J}} < 0.03$ (Haakonsen & Rutledge 2009).

The softness of the source with characteristic temperatures of a few tens of eV makes it similar to the super-soft X-ray sources (SSS; Kahabka & van den Heuvel 2006; Greiner 2000). This class of objects have BB temperatures in the range 20–100 eV, which are about two orders of magnitude lower than X-ray binaries containing an accreting NS or BH. There are various types of SSS. One main class is cooling white dwarfs (WDs; Kahabka & van den Heuvel 2006). 2XMMi J184725.1-631724 brightened by a factor of $\gtrsim 64$, thus ruling out this hypothesis. A large fraction of SSS can be interpreted as nuclear burning of the hydrogen-rich matter on the surface of a white dwarf that accretes matter from the companion, such as in the so-called close binary super-soft sources and super-soft novae (Kahabka & van den Heuvel 2006; Greiner 2000). It seems unlikely that our source is such based on the following considerations. In our Galaxy, there are only about a dozen such sources detected since the *Einstein* Observatory observations (Greiner 2000), indicating a very low density of such objects in the sky or a very low life duty cycle. The probability for any of them lying in the direction of the center of a galaxy is simply negligible. Besides, these objects are typically observed at luminosities of $\sim 10^{36} - 10^{38} \text{ ergs s}^{-1}$, while our source has much lower luminosities, $< 10^{34} \text{ ergs s}^{-1}$, if it is 5 kpc away. These objects are mostly found at distances of < 5 kpc (Greiner 2000).

5. CONCLUSION

2XMMi J184725.1-631724 is an ultrasoft X-ray transient source with characteristic temperatures of a few tens of eV. It was bright in two *XMM-Newton* observations in 2006–2007, but was not detected in a *ROSAT* pointed observation in 1992, implying a variation factor of $\gtrsim 64$ in the 0.2–10 keV absorbed flux. It was undetected again in a *Swift* observation in 2011 February, implying a flux decrease by a factor of $\gtrsim 12$. It lies toward the center of the galaxy IC 4765-f01-1504 at a redshift of 0.0353. No bright optical emission lines were detected from this galaxy, making this source a good tidal disruption event candidate. The fits to the two *XMM-Newton* spectra using a thermal disk plus a weak hard component indicate that the accretion disk luminosity appears to follow the $L \propto T^4$ relation and that the BH mass is around $10^5 - 10^6 M_{\odot}$. The source showed large fast variability in both *XMM-Newton* observations, which can be explained as due to fast variations in the mass accretion rate. To further check whether this is a tidal disruption event, future long-term X-ray monitoring is necessary to see whether it follows the decay expected for a tidal disruption event.

Acknowledgments: We thank the anonymous referee for the helpful comments. We acknowledge the use of public data from the *ROSAT*, *Swift* and *XMM-Newton* data archives, and the 2XMM Serendipitous Source Catalog, constructed by the XMM-Newton Survey Science Center on behalf of ESA. We want to thank the *Swift* PI Neil Gehrels for approving our ToO request to observe the field of 2XMMi J184725.1-631724. *Swift* is supported at PSU by NASA contract NAS5-00136. The optical spectroscopy is based on observations obtained at the Gemini Observatory which is operated by the

Association of Universities for Research in Astronomy, Inc., under a cooperative agreement with the NSF on behalf of the Gemini partnership: the National Science Foundation (United States), the Science and Technology Facilities Council (United Kingdom), the National Research Council (Canada), CONICYT (Chile), the Australian Research Council (Australia), Ministério da Ciência e Tecnologia (Brazil) and Ministerio de Ciencia, Tecnología e Innovación Productiva (Argentina). The observations were carried out as part of program GS-2011A-Q-90. SAF acknowledges funding from the Australian Research Council.

REFERENCES

- Bade, N., Komossa, S., & Dahlem, M. 1996, *A&A*, 309, L35
 Bloom, J. S., Giannios, D., Metzger, B. D., et al. 2011, *ArXiv e-prints*
 Boller, T., Brandt, W. N., & Fink, H. 1996, *A&A*, 305, 53
 Boller, T., Fabian, A. C., Sunyaev, R., et al. 2002, *MNRAS*, 329, L1
 Breeveld, A. A., Curran, P. A., Hoversten, E. A., et al. 2010, *MNRAS*, 406, 1687
 Burrows, D. N., Hill, J. E., Nousek, J. A., et al. 2005, *Space Sci. Rev.*, 120, 165
 Burrows, D. N., Kennea, J. A., Ghisellini, G., et al. 2011, *ArXiv e-prints*
 Carrasco, E. R., Mendes de Oliveira, C., & Infante, L. 2006, *AJ*, 132, 1796
 Crummy, J., Fabian, A. C., Gallo, L., & Ross, R. R. 2006, *MNRAS*, 365, 1067
 Done, C., Gierliński, M., & Kubota, A. 2007, *A&A Rev.*, 15, 1
 Esquej, P., Saxton, R. D., Freyberg, M. J., et al. 2007, *A&A*, 462, L49
 Esquej, P., Saxton, R. D., Komossa, S., et al. 2008, *A&A*, 489, 543
 Evans, C. R. & Kochanek, C. S. 1989, *ApJ*, 346, L13
 Fabian, A. C., Zoghbi, A., Ross, R. R., et al. 2009, *Nature*, 459, 540
 Farrell, S. A., Webb, N. A., Barret, D., Godet, O., & Rodrigues, J. M. 2009, *Nature*, 460, 73
 Gallo, L. C., Boller, T., Brandt, W. N., Fabian, A. C., & Grupe, D. 2004, *MNRAS*, 352, 744
 Gehrels, N., Chincarini, G., Giommi, P., et al. 2004, *ApJ*, 611, 1005
 Gezari, S., Basa, S., Martin, D. C., et al. 2008, *ApJ*, 676, 944
 Gezari, S., Halpern, J. P., Komossa, S., Grupe, D., & Leighly, K. M. 2003, *ApJ*, 592, 42
 Gezari, S., Heckman, T., Cenko, S. B., et al. 2009, *ApJ*, 698, 1367
 Gezari, S., Martin, D. C., Milliard, B., et al. 2006, *ApJ*, 653, L25
 Gierliński, M. & Done, C. 2004, *MNRAS*, 349, L7
 Goad, M. R., Roberts, T. P., Reeves, J. N., & Uttley, P. 2006, *MNRAS*, 365, 191
 Graham, A. W. 2007, *MNRAS*, 379, 711
 Greiner, J. 2000, *New Astronomy*, 5, 137
 Grupe, D., Beuerman, K., Mannheim, K., et al. 1995, *A&A*, 300, L21+
 Grupe, D., Komossa, S., Gallo, L. C., et al. 2008a, *ApJ*, 681, 982
 Grupe, D., Komossa, S., Leighly, K. M., & Page, K. L. 2010, *ApJS*, 187, 64
 Grupe, D., Leighly, K. M., & Komossa, S. 2008b, *AJ*, 136, 2343
 Grupe, D., Thomas, H., & Leighly, K. M. 1999, *A&A*, 350, L31
 Haakonsen, C. B. & Rutledge, R. E. 2009, *ApJS*, 184, 138
 Halpern, J. P., Gezari, S., & Komossa, S. 2004, *ApJ*, 604, 572
 Hill, J. E., Burrows, D. N., Nousek, J. A., et al. 2004, in *Society of Photo-Optical Instrumentation Engineers (SPIE) Conference Series*, ed. K. A. Flanagan & O. H. W. Siegmund, Vol. 5165, 217–231
 Homan, J., van der Klis, M., Jonker, P. G., et al. 2002, *ApJ*, 568, 878
 Hook, I. M., Jørgensen, I., Allington-Smith, J. R., et al. 2004, *PASP*, 116, 425
 Hyland, A. R. & Allen, D. A. 1982, *MNRAS*, 199, 943
 Jansen, F., Lumb, D., Altieri, B., et al. 2001, *A&A*, 365, L1
 Kahabka, P. & van den Heuvel, E. P. J. 2006, *Super-soft sources*, ed. Lewin, W. H. G. & van der Klis, M., 461–474
 Kalberla, P. M. W., Burton, W. B., Hartmann, D., et al. 2005, *A&A*, 440, 775
 Komossa, S. 2002, in *Reviews in Modern Astronomy*, Vol. 15, *Reviews in Modern Astronomy*, ed. R. E. Schielicke, 27–+
 Komossa, S. 2008, in *The Universe in X-rays* (eds. J. E. Trümper & G. Hasinger, Springer), 367–371
 Komossa, S. & Bade, N. 1999, *A&A*, 343, 775
 Komossa, S. & Greiner, J. 1999, *A&A*, 349, L45
 Kormendy, J. & Richstone, D. 1995, *ARA&A*, 33, 581
 Kraft, R. P., Burrows, D. N., & Nousek, J. A. 1991, *ApJ*, 374, 344
 Laor, A. & Netzer, H. 1989, *MNRAS*, 238, 897
 Lauer, T. R., Faber, S. M., Richstone, D., et al. 2007, *ApJ*, 662, 808
 Leighly, K. M. 1999a, *ApJS*, 125, 297
 —. 1999b, *ApJS*, 125, 317
 Li, L.-X., Zimmerman, E. R., Narayan, R., & McClintock, J. E. 2005, *ApJS*, 157, 335
 Lidskii, V. V. & Ozernoi, L. M. 1979, *Soviet Astronomy Letters*, 5, 16
 Lin, D., Remillard, R. A., & Homan, J. 2007, *ApJ*, 667, 1073
 —. 2009, *ApJ*, 696, 1257
 Makishima, K., Maejima, Y., Mitsuda, K., et al. 1986, *ApJ*, 308, 635
 Maksym, W. P., Ulmer, M. P., & Eracleous, M. 2010, *ApJ*, 722, 1035
 Marconi, A. & Hunt, L. K. 2003, *ApJ*, 589, L21
 Mason, K. O., Breeveld, A., Much, R., et al. 2001, *A&A*, 365, L36
 McClintock, J. E. & Remillard, R. A. 2006, *Compact Stellar X-ray Sources*, ed. W. Lewin and M. vander Klis (Cambridge: Cambridge Univ. Press), 157–213
 Miniutti, G., Fabian, A. C., Brandt, W. N., Gallo, L. C., & Boller, T. 2009, *MNRAS*, 396, L85
 Monet, D. G., Levine, S. E., Canzian, B., et al. 2003, *AJ*, 125, 984
 Peng, C. Y., Ho, L. C., Impey, C. D., & Rix, H.-W. 2010, *AJ*, 139, 2097
 Poole, T. S., Breeveld, A. A., Page, M. J., et al. 2008, *MNRAS*, 383, 627
 Puchnarewicz, E. M., Mason, K. O., Cordova, F. A., et al. 1992, *MNRAS*, 256, 589
 Rees, M. J. 1988, *Nature*, 333, 523
 —. 1990, *Science*, 247, 817
 Remillard, R. A. & McClintock, J. E. 2006, *ARA&A*, 44, 49
 Roming, P. W. A., Kennedy, T. E., Mason, K. O., et al. 2005, *Space Sci. Rev.*, 120, 95
 Ross, R. R., Fabian, A. C., & Mineshige, S. 1992, *MNRAS*, 258, 189
 Schlegel, D. J., Finkbeiner, D. P., & Davis, M. 1998, *ApJ*, 500, 525
 Schurch, N. J. & Done, C. 2007, *MNRAS*, 381, 1413
 Schurch, N. J., Done, C., & Proga, D. 2009, *ApJ*, 694, 1
 Steiner, J. F., Narayan, R., McClintock, J. E., & Ebisawa, K. 2009, *PASP*, 121, 1279
 Strüder, L., Briel, U., Dennerl, K., et al. 2001, *A&A*, 365, L18
 Tananbaum, H., Avni, Y., Branduardi, G., et al. 1979, *ApJ*, 234, L9
 Tonry, J. & Davis, M. 1979, *AJ*, 84, 1511

- Turner, M. J. L., Abbey, A., Arnaud, M., et al. 2001, A&A, 365, L27
- Turner, T. J. & Pounds, K. A. 1989, MNRAS, 240, 833
- Vasudevan, R. V. & Fabian, A. C. 2009, MNRAS, 392, 1124
- Voges, W., Aschenbach, B., Boller, T., et al. 1999, A&A, 349, 389
- Walter, R. & Fink, H. H. 1993, A&A, 274, 105
- Watson, M. G., Schröder, A. C., Fyfe, D., et al. 2009, A&A, 493, 339
- White, N. E., Giommi, P., & Angelini, L. 1994, IAU Circ., 6100, 1